



1 **Changes in the partial pressure of carbon dioxide in the Mauritanian-Cape Verde**
2 **upwelling region between 2005 and 2012.**

3

4 **By**

5

6 **Melchor González-Dávila^{1*}, J. Magdalena Santana Casiano¹ and Francisco**

7 **Machín^{1,2}**

8 ¹**Instituto de Oceanografía y Cambio Global, Grupo QUIMA, Universidad de Las**

9 **Palmas de Gran Canaria, 35017, Las Palmas de Gran Canaria. Spain.**

10 ²**Departamento de Física, Universidad de Las Palmas de Gran Canaria, 35017, Las**

11 **Palmas de Gran Canaria**

12

13

14 * Correspondence to melchor.gonzalez@ulpgc.es

15

16



17 **ABSTRACT**

18 Coastal upwelling along the eastern margins of major ocean basins represent regions of
19 large economic importance due to the high biological productivity. However, the physical
20 forcing of upwelling processes that favor the production in these areas are being affected
21 by global warming, which will modify the intensity of the upwelling and, consequently,
22 the carbon dioxide cycle. For this reason, the role of observations in addressing any
23 climate change impacts on the global carbon cycle in areas of upwelling is of great
24 importance. Monthly high resolution surface experimental data for temperature and
25 partial pressure of carbon dioxide in the Mauritanian-Cape Verde upwelling region from
26 2005 to 2012 are shown. This data set provides direct evidence of seasonal and
27 interannual changes in the physical and biochemical processes. They confirmed an
28 upwelling intensification and an increase in the CO₂ outgassing of 1 Tg a year in one of
29 the four most important upwelling regions of the planet due to wind increase, even when
30 primary production seems to also be reinforced. This increase in CO₂ intake together with
31 the observed decrease in sea surface temperature at the location of the Mauritanian Cape
32 Blanc, 21°N, produced a pH decrease of -0.003 ± 0.001 per year.

33



34 **1. INTRODUCTION**

35

36 The excess of CO₂ in the atmosphere, largely responsible of Global Climate Change, has
37 prompted research on the role of the oceans in the carbon cycle. In recent decades data
38 from different oceans have been taken as thoroughly as possible, with the aim to assess
39 how the oceans act as sources or sinks within the carbon cycle. To achieve this goal,
40 observations representative of the distribution of CO₂ fluxes between the ocean and
41 atmosphere are necessary. In this regard, automated instruments have been installed on
42 opportunity ships for sampling the ocean as much as possible, data is being collected at
43 scientific cruises and long-term moorings have been deployed in various sites of the
44 oceans (i.e., Astor et al., 2005; Lüger et al., 2004, 2006; González-Dávila et al., 2005;
45 2009; Schuster et al., 2009; Ullman et al., 2009; Watson et al., 2009; Padín et al., 2010;
46 Gruber et al., 2002; Dore et al., 2003; Santana-Casiano et al., 2007; Bates et al., 2014).

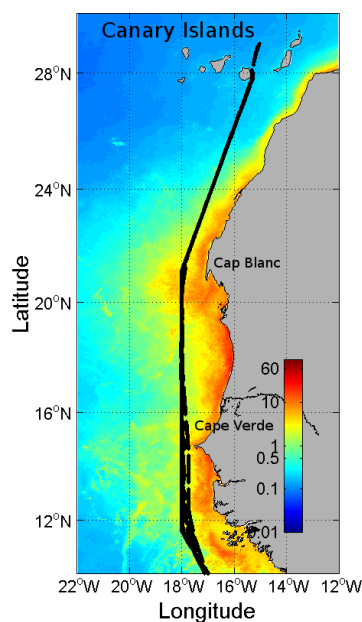
47 With the amount of data already gathered (<http://www.socat.info/>), climatologies that
48 present average fluxes between the atmosphere and the ocean have been developed, so
49 areas acting as a source or sink are now identified (Key et al., 2004; Takahashi et al.,
50 2009). However, the low spatial resolution of these databases makes it lose relevant
51 variability at relatively low spatial scales. This occurs in coastal areas, specially in
52 upwelling regions, which are not adequately represented in large databases. Upwelling
53 zones present a dynamic that raises water from relatively deep areas, which are rich in
54 nutrients and CO₂. Nutrients promote primary production, which consumes CO₂, a
55 process that would generate a CO₂ flux into the ocean. On the other hand, the upwelling
56 also brings up CO₂ from deep seawater, which finally generates uncertainty about the
57 actual role of upwelling areas as a source or sink of CO₂ (Michaels *et al.*, 2001). Indeed,
58 previous researches indicate that upwelling areas act as a source or sink of CO₂ depending



59 on their location (Cai *et al.*, 2006; Chen *et al.*, 2013), where upwelling areas at low
60 latitudes mainly act as a source of CO₂ (Feely *et al.*, 2002; Astor *et al.*, 2005; Friederich
61 *et al.*, 2008; Santana-Casiano *et al.*, 2009; González-Dávila *et al.*, 2009) and those at mid-
62 latitudes act as a sink of CO₂ (Frankignoulle and Borges, 2001; Hales *et al.*, 2005; Borges
63 *et al.*, 2002; 2005; Santana-Casiano *et al.*, 2009; González-Dávila *et al.*, 2009). Several
64 anthropogenic interactive effects are strongly influencing the general picture for the most
65 representative Eastern Boundary Upwelling Systems (EBUS), and include upper ocean
66 warming, ocean acidification and ocean deoxygenation (Gruber, 2011; Feely *et al.*, 2008;
67 Keeling *et al.*, 2010). Moreover, evidence for an increase in winds that favor upwelling
68 (Bakun, 1990; Demarcq, 2009; Oerder *et al.* 2015) support the possibility of a change in
69 the current role of these highly productive areas. Recently, eddy-resolving regional ocean
70 models have shown how upwelling intensification can be followed by major impact on
71 the system's biological productivity and in the CO₂ outgassing (Lachkar and Gruber,
72 2013; Oerder *et al.*, 2015). Wind observations and reanalysis products are controversial
73 regarding the Bakun intensification hypothesis (Bakun 1990). Using different winds
74 database for the Canary region, Barton *et al.* (2013) concluded that there was no evidence
75 for a general increase in the upwelling intensity off northwest Africa. Marcello *et al.*
76 (2011) found an intensification of the upwelling system in the same area during a 20-year
77 period while the alongshore wind stress remained almost stable. Cropper *et al.* (2014)
78 found that coastal summer wind speed increased, resulting in an increase in upwelling-
79 favorable wind speeds north of 20°N and an increase in downwelling-favorable winds
80 south of 20°N. Santos *et al.* (2005; 2012) showed differences in Sea Surface Temperature,
81 SST, between coast and ocean depending on the upwelling index, UI intensity, and that
82 SST trends were not homogeneous either along latitude or longitude. Varela *et al.* (2015)
83 also showed opposite results world wide when different wind databases were used and



84 when the same wind database was considered depending on the length of data, season
85 evaluated, and selected area. For the Mauritanian region, when wind stress data were used
86 (Varela et al., 2015), a more persistent increasing trend in upwelling-favourable winds
87 north of 21°N and a decreasing trend south of 19°N were determined.
88 Starting in June 2005, the QUIMA-voluntary opportunity ship line visited the
89 Mauritanian-Cape Verde upwelling region northwest of Africa on a monthly basis (Fig.
90 1 and Supplementary Table 1S) producing for the first time a high resolution SST and
91 partial pressure of CO₂, *f*CO₂, database. This database has been considered to show the
92 variations in the CO₂ system under changes in the upwelling conditions in the Canary
93 Ecosystem from 27°N to 10°N for the period 2005 to 2012.



94 Fig. 1. Ship track in the area from 28°N (Gran Canaria, The Canary Islands) to 10°N (black dots).
95 The locations of Cap Blanc and Cape Verde are indicated. Monthly Ocean Color
96 (oceancolor.gsfc.nasa.gov) data for average chlorophyll *a* concentration (mg m⁻³) were included
97 in a Matlab™ routine and annually averaged, in order to draw the map for the area. The map has
98 been generated using Matlab 7.12 R2011a.
99



100 **2. EXPERIMENTAL**

101 **2.1 Region evaluated.**

102 The VOS line crosses the East Atlantic Ocean from the north of Europe (English Channel)
103 to South Africa, calling Gran Canaria, the Canary Islands, with a periodicity of two
104 months, which provides monthly data (southward or northward sections). In this work,
105 the area between Gran Canaria at 27°N and 10 °N has been selected in order to study the
106 Mauritanian-Cape Verde upwelling region. In its south route (Fig. 1), the ship leaves
107 Gran Canaria, and goes straight to 100 Km off Cap Blanc, at 21°N 17°45'W. It then
108 follows this longitude, passing at 100 km off Cape Verde until 12°N, where it changes
109 direction to Cape Town, reaching 10°N 17°W at 330 km out of the coast of Guinea.
110 Between 22°N and 20°N, the ship reaches the 500 m isobath. South of 15°N, the ship
111 moves between 1000 and 500 m isobath. In its north route, the ship follow the same
112 reverse track.

113 **2.2 Experimental data**

114 Experimental data were obtained under the EU projects Carbocean and Carbochange
115 (www.CarboOcean.org, <https://carbochange.b.uib.no/>) and now also available at
116 <http://www.socat.info/>. An autonomous instrument for the determination of the partial
117 pressure of CO₂ developed by Craig Neill following NOAA recommendations was
118 installed in opportunity ships operated by the MSC company during the 2005 to 2008
119 period and Maersk Company from 2010 to 2012 along the so called QUIMA-VOS line
120 between the UK and Cape Town, from July 2005 to January 2013 (Supplementary
121 Table S1). Temperature was measured at three locations along the sampling circuit: in the
122 intake (SeaBird SBE38L), in the equilibrator (SeaBird thermosalinograph SBE21 and
123 internal PT100 thermometer), and in the oxygen sensor (Optode 3835 Aanderaa™).
124 Differences between equilibrator and intake were constant in time due to the high



125 seawater flux used but varied among ships due to the different locations of the equipment.
126 Values varied between 0.06°C when the equipment was placed close to the intake to
127 0.35°C, when the equipment was one floor above, inside the engine room. The SST was
128 also obtained from the NOAA_OI_SST-V2 data provided by the NOAA/OAR/ESRL
129 PSD, Boulder, Colorado, USA (<http://www.esrl.noaa.gov/psd>). These data had a spatial
130 resolution of 1° latitude and 1° longitude and monthly averages were used. The correlation
131 between our experimental SST data and satellite one was better than $\pm 1^\circ\text{C}$, and reduced
132 to $\pm 0.4^\circ\text{C}$ after removing the most affected upwelling regions (19-22°N and 14-16°N),
133 related to the high variability imposed by the upwelling.

134 The CO_2 molar fraction, $x\text{CO}_2$, in seawater was obtained every 150 s, while
135 atmospheric $x\text{CO}_2$ data were taken every 200 min. The seawater intake was located at a
136 10 m depth. The system was calibrated every three hours, by measuring four different
137 standard gases with mixing ratios of 0.0, 250 ppm, 380 ppm and 490 ppm of CO_2 in the
138 air, provided by NOAA and traceable to the World Meteorological Organisation scale.
139 The precision of the system is greater than 0.5 μatm and the accuracy estimated with
140 respect to the standard gases is of 1 μatm . The fugacity of CO_2 , $f\text{CO}_2$ (μatm), was
141 calculated from $x\text{CO}_2$ after correcting for temperature differences between intake and
142 equilibrator, according to the expressions for the seawater given by DOE (1994).

143 In order to compute a second carbonate system variable, the surface total alkalinity
144 was computed from sea surface salinity, SSS, and SST (Lee et al., 2006). pH_T at the in
145 situ temperature was computed from $f\text{CO}_2$ and A_T and with average annual surface ocean
146 total phosphate and total silicate concentrations of 0.5 and 4.8 $\mu\text{mol kg}^{-1}$, respectively,
147 from the World Ocean Atlas 2009, using the carbonic acid acidity constants by Merbach
148 et al (1973) refitted by Dickson and Millero (1987).

149 Air-sea CO_2 fluxes, FCO_2 ($\text{mmol m}^{-2} \text{d}^{-1}$), were evaluated as



$$150 \quad FCO_2 = 0.24 * k * s * (fCO_2^{sw} - fCO_2^{atm}) \quad (1)$$

151 where 0.24 is the scale factor, k is the gas transfer velocity, s is the CO₂ solubility, fCO_2^{sw}
 152 is the seawater fugacity of CO₂ and fCO_2^{atm} is the atmospheric fugacity of CO₂. In order
 153 to evaluate ΔfCO_2 ($\Delta fCO_2 = fCO_2^{sw} - fCO_2^{atm}$), fCO_2^{atm} data were linearly interpolated to
 154 the fCO_2^{sw} time vector. A positive value for FCO_2 corresponds with a CO₂ outgassing
 155 from the ocean. k (cm h⁻¹) was evaluated with the parametrization (Wannikhoff, 1992):

$$156 \quad k = 0.31 * W^2 * (Sc/660)^{-1/2} \quad (2)$$

157 where W is the wind speed at 10 m above the sea surface (m s⁻¹) and Sc is the Schmidt
 158 number.

159 The variables involved in estimating FCO_2 data (i.e. fCO_2^{sw} , fCO_2^{atm} , SST and SSS)
 160 were fitted to sinusoidal expressions (Lüger et al., 2004) for a given latitude as:

$$161 \quad X(lat)^* = a_0 + a_1(t - 2005) + a_2 \sin(2\pi t) + a_3 \cos(2\pi t) + a_4 \sin(4\pi t) +$$

$$162 \quad a_5 \cos(4\pi t) \quad (3)$$

163 where a_i are the fitting coefficients, t is the sampling time expressed as year fraction and
 164 X represents any of the four variables. This procedure allowed us to re-construct the series
 165 of experimental data for periods not properly sampled. The variables were decomposed
 166 into an interannual term $X(lat)_t^* = a_0 + a_1(t - 2005)$ plus a periodical term $X(lat)_p^* =$
 167 $a_2 \sin(2\pi t) + a_3 \cos(2\pi t) + a_4 \sin(4\pi t) + a_5 \cos(4\pi t)$, that is, $X(lat)^* = X(lat)_t^* +$
 168 $X(lat)_p^*$. The periodical term accounts for the high frequency seasonal variability, while
 169 the interannual one marks the year-to-year trend. First, observations were grouped in a
 170 natural year for a given latitude, as if they had been taken in a single year (no correction
 171 was done for interannual variability). The mean seasonal climatology data associated with
 172 the periodic coefficients (i.e. a_2 , a_3 , a_4 , and a_5) throughout the sampling period were
 173 determined. Next, the interannual coefficients a_1 were calculated by fitting the residuals
 174 resulting from subtracting the periodical component, $X(lat)_p^*$, from the original variable



175 $X(lat)$. Fixing these five coefficients (a_1 - a_5), new distributions for fCO_2^{sw*} , fCO_2^{atm*} , $temp^*$
176 and $salinity^*$ were constructed with a daily resolution based on the curve fits given for
177 each variable as in Eq. (3), providing the coefficient a_0 . The mean residual on the
178 determination of those four variables with respect to the experimental values were ± 3.7
179 μatm , $\pm 1.5 \mu atm$, $\pm 0.22 \text{ }^\circ C$, and ± 0.05 for fCO_2^{sw*} , fCO_2^{atm*} , $temp^*$ and $salinity^*$,
180 respectively. When the monthly satellite SST values were considered, the new $temp^*$
181 function averaged for each month produced values within $\pm 0.47^\circ C$, confirming that this
182 procedure was able to fit non-sampled periods. It was assumed that the same procedure
183 was valid for non-sampled fCO_2 . Finally, daily fCO_2^* time series between 10 and $27^\circ N$
184 with a latitudinal resolution of 0.5° were calculated with a standard error of estimation of
185 $0.5 \text{ mmol m}^{-2} \text{ d}^{-1}$ (15% of error) that produced mean residuals (experimental fCO_2 -
186 fCO_2^*) of $0.4 \text{ mmol m}^{-2} \text{ d}^{-1}$ and Pearson correlation coefficients between experimental
187 and computed fCO_2^* of $r > 0.6$, $p < 0.01$.

188 Chlorophyll-a was calculated from measurements made by the Moderate Resolution
189 Imaging Spectroradiometer (MODIS) aboard NASA's Aqua satellite. Monthly averages
190 with spatial resolution of 9 km supplied by Ocean Color (oceancolor.gsfc.nasa.gov) were
191 used.

192 Wind data were downloaded from the NCEP CFSR database at
193 <http://rda.ucar.edu/pub/cfsr.html> developed by NOAA and retrieved from the NOAA
194 National Operational Model Archive and Distribution System and maintained by the
195 NOAA National Climatic Data Center. The spatial resolution is approximately $0.3 \times 0.3^\circ$
196 and the temporal resolution is 6 hours. The reference height of the wind data is 10 m.

197 Rainfall data were collected by the Precipitation Radar installed on the Tropical
198 Rainfall Measuring Mission (TRMM) satellite (<http://precip.gsfc.nasa.gov>). Monthly
199 averages with a spatial resolution of $0.5^\circ \times 0.5^\circ$ (product 3A12, version 07) were used



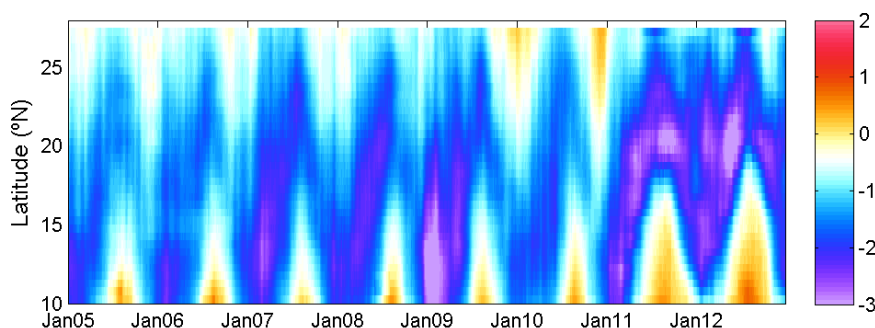
200 (Supplementary Fig. S1) in order to explain changes in seasonal surface salinity
201 distributions.

202

203 3. RESULTS AND DISCUSSION

204 3.1 Physical properties

205 The variability of the Mauritanian-Cape Verde upwelling was analyzed in terms
206 of the upwelling index (Nykjaer and Van Camp, 1994) (Fig. 2) using satellite wind data.

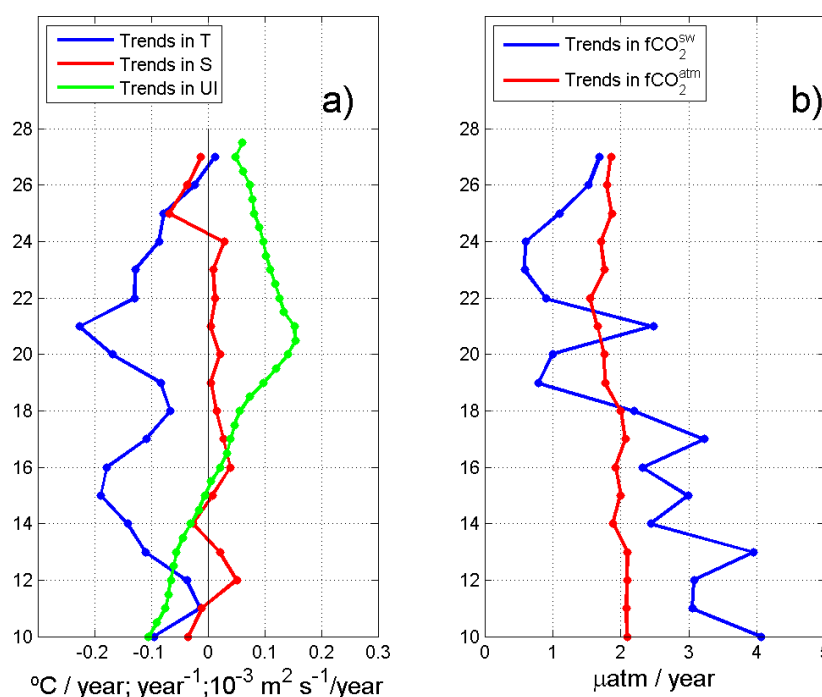


207 Fig. 2. Time series of upwelling index ($\text{m}^2 \text{s}^{-1}$) in the Mauritanian-Cape Verde upwelling region
208 along the ship track computed following Nykjaer and Van Camp (1994).
209

210 Results clearly distinguish two main subareas in the upwelling system. 1) North
211 of 20°N , the upwelling conditions were favorable throughout the year, although the
212 highest upwellings were observed from March to September with a northward shift from
213 20° to 22°N . 2) South of 20°N , a marked seasonality was observed. South of 15°N , in the
214 Cape Verde area, upwelling conditions were favorable during autumn and winter with the
215 maximum intensity observed during January and February due to the replacement of the
216 trade winds during the summer by the monsoon winds, which advect warm water
217 northward along the shore (Nykjaer and Van Camp, 1994). Our results (Fig. 2) are quite
218 consistent with previous research (Nykjaer and Van Camp, 1994; Marcello et al., 2011;
219 Santos et al., 2005; 2012) but include the years 2010 to 2012 where UI at around $20\text{-}21^\circ\text{N}$



220 presented a shift of the upwelling regime intensity from high to strong. The analysis of
 221 upwelling trends along this area has been controversial since it is highly dependent on the
 222 selected region (Santos et al., 2012). The inter-annual evolution of UI over the period
 223 2005 to 2012 (Fig. 3, green line) determined by averaging monthly values on an annual
 224 base followed that showed by Santos et al. (2012), indicating an increase in the UI (mean
 225 confidence interval of $9 \text{ m}^2 \text{ s}^{-1}$).



226 Fig. 3. Latitudinal distribution of the interannual trends for the Upwelling Index (UI) and for the
 227 four experimental variables along the QUIMA-VOS line integrated over every degree. The a)
 228 panel presents the trends for Upwelling index (mean confidence interval of $9 \text{ m}^2 \text{ s}^{-1}$), SST ($^{\circ}\text{C}$
 229 yr^{-1} , confidence interval 0.13°C) and SSS (yr^{-1} , confidence interval 0.06) and the b) panel the
 230 trends for $f\text{CO}_2^{\text{sw}}$ and $f\text{CO}_2^{\text{atm}}$ (confidence intervals 4.23 and $0.44 \mu\text{atm}$).
 231

232

233 The upwelling index (except for the area south of 15°N) confirmed the stronger
 234 upwelling observed since 1995-1996 in this region after a more than a 10-year (from at
 235 least 1982 to 1995) period of weaker upwelling (Santos et al., 2012). Local zonal



236 differences between ocean and coastal SST trends determined by using satellite data by
237 Santos et al. (2005) for the period 1982 to 2000, extended by Santos et al. (2012) until
238 2010 and in this study until 2012 (data not shown) confirmed the intensification of the
239 upwelling regime along the African coast. This has been described as a decadal scale shift
240 of the upwelling regime intensity (Marcello et al., 2011; Santos et al., 2012). To the south
241 of 15°N, the annual UI values (Fig. 2 and 3) indicate that the SST close to the coast is
242 becoming warmer. They serve as an indication of decadal variability of the summer
243 monsoon winds and associated northward advection of warm water along the coast
244 (Santos et al., 2012). The highest upwelling intensity along the VOS line was located at
245 the capes, Cap Blanc and Cape Verde. From satellite chlorophyll-*a* data, especially off
246 Cap Blanc, giant filaments with chlorophyll concentrations above 1 mg m⁻³ persist year-
247 round, spreading from the coast several hundred kilometers offshore (Fig. 1). North of
248 Cap Blanc the upwelled water originates from the North Atlantic Central Water, and
249 mixes with South Atlantic Central Water, SACW, towards the south (Mittelstaedt, 1983).
250 South of Cap Blanc, the upwelling of nutrient rich SACW promotes phytoplankton
251 growth between Cap Blanc and Cape Verde. Towards 12°N, upwelling is also fed by the
252 North Equatorial Under Current (Hagen and Schemainda, 1984). Moreover, the entire
253 northwest African coast is also influenced by the African desert dust transport by the mid-
254 tropospheric Harmattan winds originating from the central Sahara, which supplements
255 the levels of micronutrients (such as iron) to the adjacent marine ecosystem (Mittelstaedt,
256 1983; Neuer et al., 2004; Swap et al., 1996).

257 The area is also affected by the migration of the Inter-Tropical Convergence Zone
258 (ITCZ), related to maximum precipitation rates. To have a significant satellite
259 precipitation record in our region of interest, precipitation data were integrated
260 longitudinally between 25.25°W and 9.75°W. Time series for the latitudinal distribution

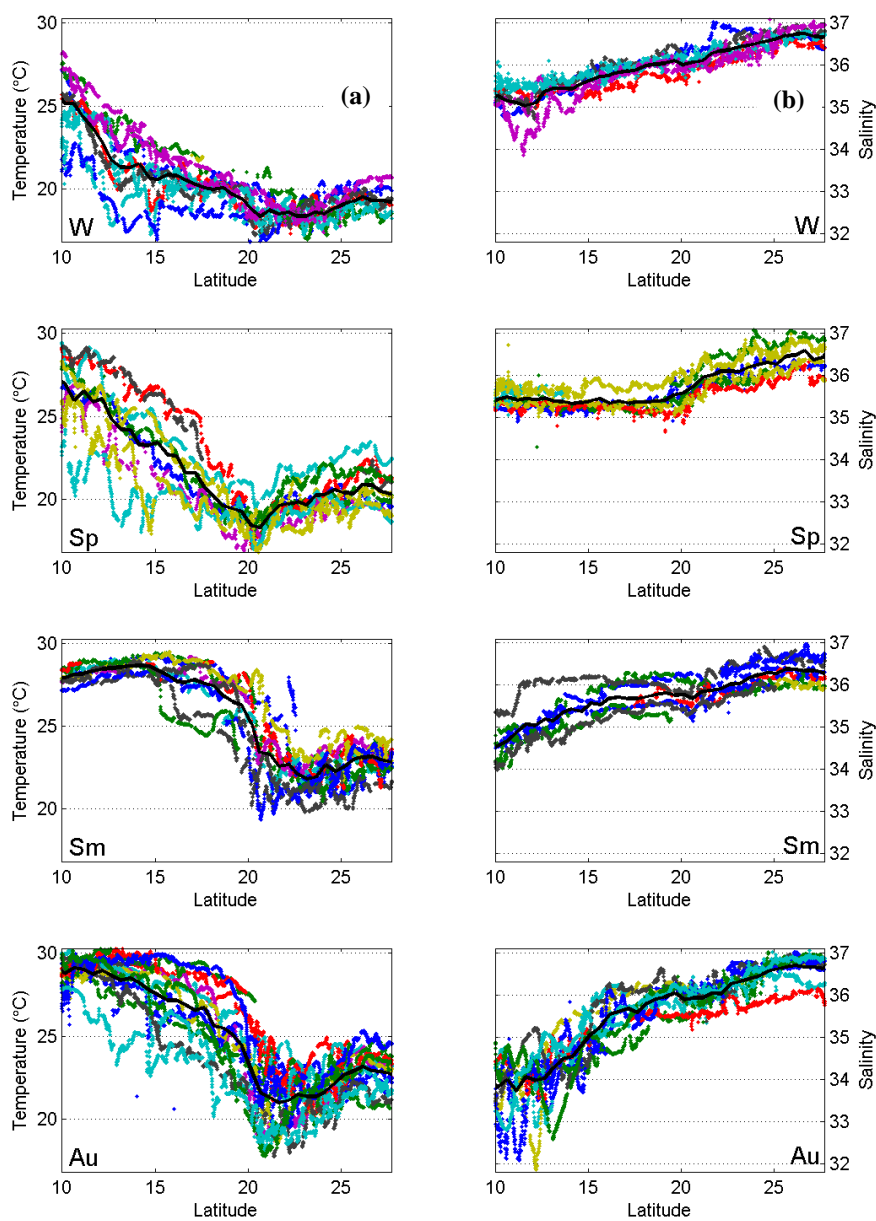


261 of integrated precipitation (Supplementary Fig. 1S) identified the average position of the
262 ITCZ related to maximum precipitation rates. The ITCZ was located at its southernmost
263 position (2°N) during winter, reaching its northernmost position (14-16°N) around
264 summer. The ITCZ reached our area of interest (>10°N) from late spring to late summer.

265 The latitudinal distributions of experimental surface temperature and salinity
266 along the vessel track are shown in Fig. 4, grouped by seasons. In situ temperature at
267 27°N shows temperatures in the range of 18 to 24°C with the minimum in winter and
268 maximum in late summer-early autumn. The annual temperature range was somewhat
269 higher at 20°N, with summer maximum of around 26°C and minimum in spring of about
270 17°C. At 10°N, temperatures were the highest throughout the year (>25°C), with
271 minimum values in winter and maximum in late spring and late autumn. The low values
272 observed during the end of summer are related to the arriving of the ITZC at those
273 latitudes. The thermal distribution shows a temperature increase as we move to the
274 Equator and a notable cooling at the upwelled waters off Mauritania. The temperature
275 generally decreased from 10°N to about 20°N to 21°N, where the ship meets the
276 Mauritanian upwelling. From there to the north, the temperature rises as the ship leaves
277 the upwelling area on its way to the Canary Islands. Only during winter time and the
278 beginning of the spring, the upwelling of cold water from Cape Verde area was detected.
279 Salinity minimum values were normally located at 10°N, increasing to maximum values
280 at the Canaries' latitude. The minimum values of salinity were exceptionally low during
281 autumn from 10°N to 16°N by both the freshwater input from rivers that increase their
282 outflow during this season (Nicholson, 1981) and by the northward shift of the ITCZ
283 during this part of the year.

284

285



286 Fig. 4. Experimental series of a) SST and b) SSS data in the Mauritanian - Cape Verde coastal
287 region grouped by seasons: winter (W), spring (Sp), summer (Sm) and autumn (Au). The averaged
288 values for all cruises in Table S1, are shown in black for each season including the 95%
289 confidence limits.

290

291 Anomaly fields for temperature and salinity (data not shown) were calculated as

292 the difference between the observations and the mean values at each season for individual

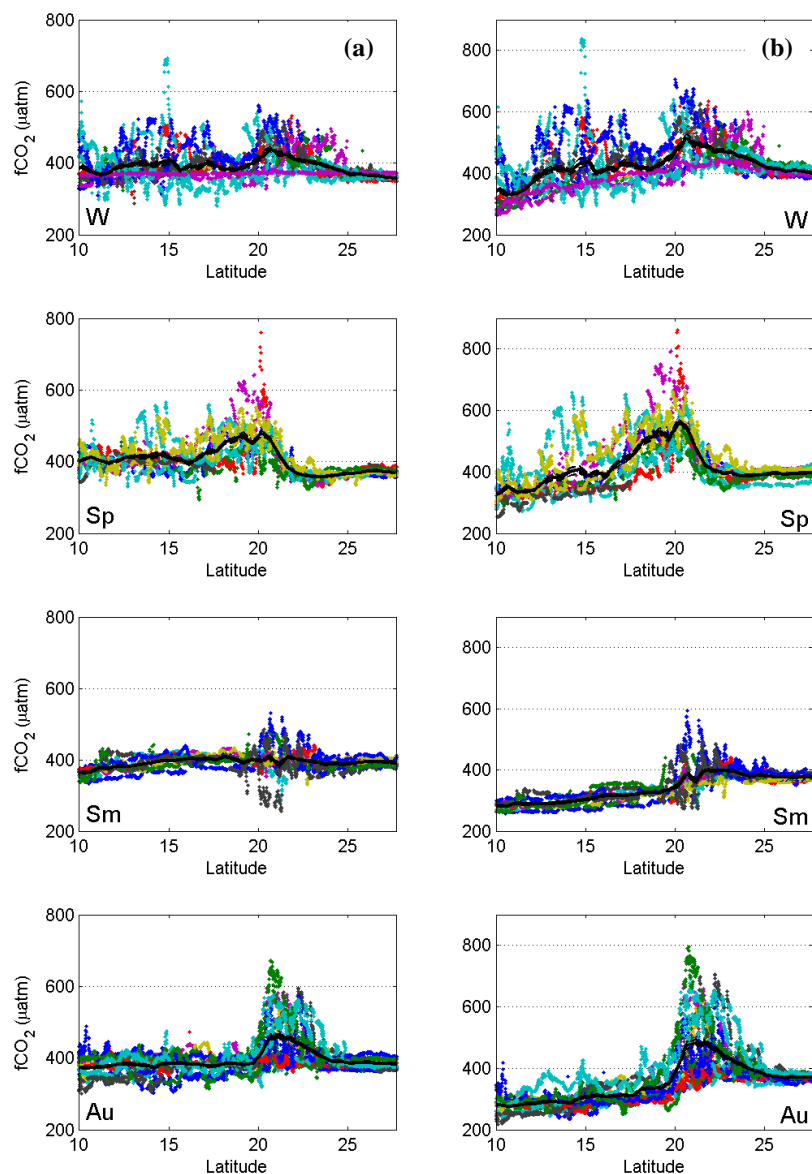


293 latitudes. For temperature, the largest anomalies in winter and spring were located south
294 of 18°N, with values of $\pm 2^\circ\text{C}$, related to the seasonal cycle of the Cape Verde upwelling.
295 During summer the pattern changed and the largest anomalies were detected in the
296 upwelling area at 18-22°N, with values of $\pm 5^\circ\text{C}$ when the upwelling index for the
297 Mauritanian area was highest (Fig. 2). In autumn the temperature anomalies were shifted
298 slightly to the north, 20-24°N, with values of $\pm 3^\circ\text{C}$ related to the observed pulses in
299 upwelling favorable winds that affected the surface seawater properties. On the other
300 hand, salinity anomalies showed a very homogeneous pattern in all latitudes for winter,
301 spring and summer, with values generally within ± 0.5 . However, during autumn
302 important anomalies south of 18°N were observed, with values in the range of ± 1.5 . In
303 this region, the upwelling development, the river discharge and the rainy season
304 controlled the observed distribution (Yoo and Carton, 1990).

305

306 **3.2 Carbon dioxide variability**

307 The latitudinal distribution of the experimental $f\text{CO}_2^{\text{sw}}$ data (Fig. 5a) grouped by
308 seasons, showed they were always above the $f\text{CO}_2^{\text{atm}}$, with the highest values between
309 18 and 23°N for all seasons due to the variability imposed by the upwelling off
310 Mauritania. During winter, when the Cape Verde upwelling develops (Fig. 2), the 12-
311 15°N region also presented higher $f\text{CO}_2^{\text{sw}}$ values than those in the atmosphere. $f\text{CO}_2^{\text{sw}}$
312 data showed a latitudinal shift along the seasons following that observed in the upwelling
313 index: i.e., in winter, the largest values were located between 19° and 24°N; in spring,
314 they were located between 16° and 22°N; during summer and autumn, the largest $f\text{CO}_2^{\text{sw}}$
315 values were recorded in the range 20° to 23°N. $f\text{CO}_2^{\text{sw}}$ normalized to the mean SST of
316 22°C for the region ($N/f\text{CO}_2^{\text{sw}}$, Fig. 5b) reinforced the variability indicating that upwelling
317 is the major factor contributing to the $f\text{CO}_2$ variability.



318 Fig 5. Experimental series of fugacity of CO₂ data in the Mauritanian-Cape Verde coastal region
319 grouped by seasons: winter (W), spring (Sp), summer (Sm) and autumn (Au). a) $f\text{CO}_2^{\text{sw}}$ latitudinal
320 distribution. b) Normalized $f\text{CO}_2^{\text{sw}}$ values to a constant temperature of 22°C. The averaged values
321 for all cruises in Table S1, are shown in black for each season including the 95% confidence
322 limits.
323

324 According to Takahashi et al. (1993), $f\text{CO}_2^{\text{sw}}$ increases with temperature at a rate
325 that is 4.3% $\mu\text{atm } ^\circ\text{C}^{-1}$ (around 16 $\mu\text{atm } ^\circ\text{C}^{-1}$ at this area) in a thermodynamically controlled



326 system. At 27°N, the rate, as SST increases, was only of 7.45 $\mu\text{atm } ^\circ\text{C}^{-1}$ due first to
327 biological uptake and second to the CO_2 outflux. At 20°N the rate became negative with
328 a value of $-10.9 \mu\text{atm } ^\circ\text{C}^{-1}$, clearly indicating the important injection of cool and CO_2 rich
329 seawater at the upwelling area, neither being compensated by the solubility nor the
330 biological carbon pumps. At 10°N, and as a result of the seasonal upwelling, the rate was
331 still negative but of only $-4.3 \mu\text{atm } ^\circ\text{C}^{-1}$. When $N_f\text{CO}_2^{\text{sw}}$ was related with SST at the
332 latitudes 19° to 21°N in the upwelling vicinity of Cap Blanc, an inverse relationship of
333 $70\text{-}100 \mu\text{atm } ^\circ\text{C}^{-1}$ was found during winter and spring, while in summer and autumn the
334 inverse relationship was reduced to $12\text{-}18 \mu\text{atm } ^\circ\text{C}^{-1}$. While the upwelling indexes at those
335 latitudes were quite constant throughout the year, the different rates observed should be
336 related to biological consumption of the CO_2 excess. During winter and spring the
337 injection of CO_2 in the upwelling is not decreased by the biological activity in the area.
338 At the end of spring and during summer the Chl-*a* content reached its maximum and most
339 of the CO_2 was consumed and/or exported and, therefore, the rate was strongly reduced.

340 Figure 3 depicts the observed interannual trends (a_1 coefficient in Eq. 3) for the
341 four experimental recorded detrended parameters, together with the UI trend. Confidence
342 intervals of the computed mean annual values for SST, SSS, $f\text{CO}_2^{\text{atm}}$, $f\text{CO}_2^{\text{sw}}$ were 0.13°C ,
343 0.06 , $0.44 \mu\text{atm}$ and $4.23 \mu\text{atm}$, respectively. There was a clear SST trend whereby
344 seawater along the VOS line track was getting cooler with maximum cooling rates at the
345 location of Cap Blanc (21°N) and Cape Verde upwellings (15°N) with rates higher than -
346 $0.2^\circ\text{C yr}^{-1}$. Data from the first three years (2005 to 2008) at 21°N showed lower
347 temperatures with higher cooling rates that reached $-0.7^\circ\text{C yr}^{-1}$, although three years of
348 data are not representative. The area crossed by the VOS line along $17^\circ45'\text{W}$ from 22°N
349 to 10°N is located inside the 1000 m isobath that is well inside the mean frontal activity
350 in the Canary region of about 200 km width (Wang et al., 2015). The different changes



351 in temperature in the coastal slope and offshore waters are related to the different origins
352 of the waters upwelled from depths of about 100 m to the surface (Mittelstaedt, 1983)
353 that spread off the coastal area. The offshore water SST is less variable owing to longer
354 residence time in the ocean surface. These effects and the fact that the VOS line keeps a
355 track line that crossed the upwelling cells at a distance to the coast that varies among cells,
356 contributes to the observed spatial variability. There was no attempt to compare
357 latitudinal and longitudinal effects on the observed values. Our experimental data,
358 however, does not show any positive annual based SST rates in the upwell affected area,
359 and only when the ship approached the Canary Islands, the trends became less negative,
360 reaching a value of $+0.02^{\circ}\text{C yr}^{-1}$ at 27°N , similar to those obtained for oceanic Atlantic
361 water (Bates et al., 2014).

362 $f\text{CO}_2^{\text{atm}}$ for the area presented the interannual increase of about $2 \pm 0.3 \mu\text{atm y}^{-1}$
363 observed in atmospheric stations, while $f\text{CO}_2^{\text{sw}}$ presented a heterogeneous distribution.
364 South of 18°N the rate of increase was always higher than that in the atmosphere reaching
365 a maximum value of $4.1 \pm 0.4 \mu\text{atm y}^{-1}$ at 10°N . At 27°N , $f\text{CO}_2^{\text{sw}}$ increased at a rate of
366 $1.7 \pm 0.2 \mu\text{atm y}^{-1}$ similar to that determined at the ESTOC time series site (González-
367 Dávila et al., 2010) located at $29^{\circ}10' \text{ N } 15^{\circ}30' \text{ W}$. In the Cap Blanc area, $f\text{CO}_2^{\text{sw}}$ increased
368 at an average rate of $2.5 \pm 0.4 \mu\text{atm y}^{-1}$ with the highest values in the period 2005 to 2008
369 (a rate of $4.6 \pm 0.5 \mu\text{atm y}^{-1}$ was computed with only those years). Around Cap Blanc,
370 $f\text{CO}_2^{\text{sw}}$ always presented lower rates of increase than in the atmosphere with values well
371 below $1 \mu\text{atm y}^{-1}$. The observed decrease in SST and the trends in $f\text{CO}_2^{\text{sw}}$ can only be
372 explained by a reinforced upwelling. North of 18°N , the lowest rate of increase in $f\text{CO}_2^{\text{sw}}$
373 compared to $f\text{CO}_2^{\text{atm}}$, together with a decrease in temperature, indicated that upwelling is
374 also favoring an increase in the net community production around the Mauritanian
375 upwelling, consuming and/or exporting the CO_2 rich upwelled waters favored by the

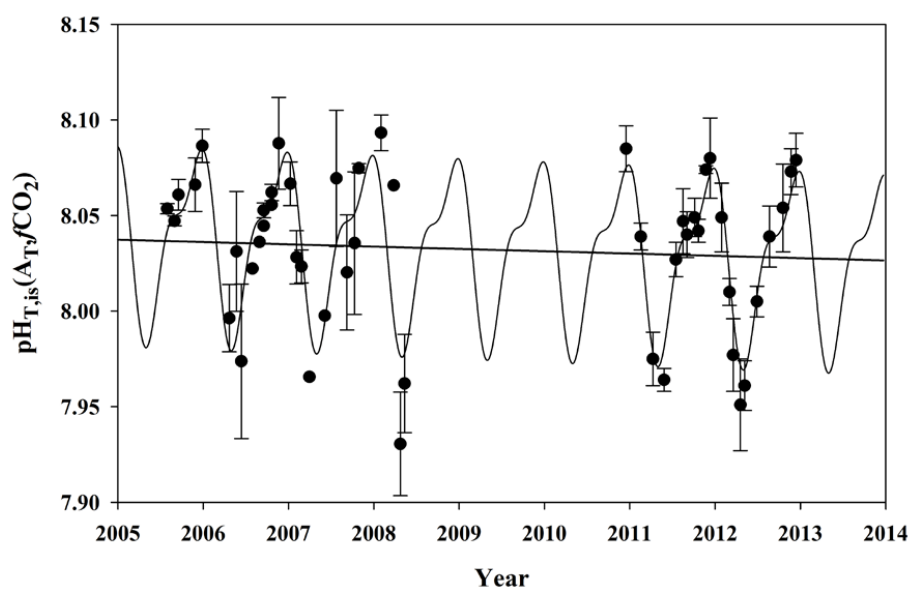


376 lateral transport of the Mauritanian current (Lachkar and Gruber, 2013; Varela et al.,
377 2015). The upwelling intensification effects observed in the trends of our experimental
378 data support the recent wind stress trends (Crooper et al., 2014; Varela et al., 2015; Santos
379 et al., 2012) of increased upwelling-favorable winds, at least for the period 2005-2012 in
380 the Canary upwelling region (Fig. 2 and 3). The intensification of the upwelling results
381 in a change in the measured upwelled water properties due to either higher upwelling
382 velocities or deeper source upwelled waters. However, what remains unclear from these
383 records is to what extent those changes reflect upwelling variations due to climate change
384 forcing versus natural decadal variability in the upwelling areas occurring over
385 interannual timescales.

386 Because of the upwelling intensity is changing, other variables will also be
387 affected. $\text{pH}_{\text{T, is}}$ at $21 \pm 0.25^\circ\text{N}$ was computed from $f\text{CO}_2$ and alkalinity pairs of data.
388 Alkalinity was computed from regional correlations with SST and SSS (Lee et al., 2006)
389 which could under-represent seasonal and interannual variations in upwelling areas.
390 However, pH computed from $f\text{CO}_2$ values are relatively insensitive to errors in A_{T} , and
391 $f\text{CO}_2$ controls the magnitude and variability of pH (a $60 \mu\text{mol kg}^{-1}$ change in A_{T} will affect
392 a 0.1% in pH, that is, about 0.01 pH units). Figure 6 depicts the computed $\text{pH}_{\text{T, is}}(A_{\text{T}}, f\text{CO}_2)$
393 data and the harmonic fitting Eq. (3) providing seasonal variability and interannual trend.
394 Considering the small systematic biases in interannual dynamics, it is determined a
395 decrease in pH at a rate of -0.003 ± 0.001 per year (Fig. 6). This decrease is on the highest
396 rate values determined in several time series stations (Bates et al., 2014), where oceanic
397 SST has only slightly increased in the last decades. However, at the Mauritanian
398 upwelling area and at the location where our VOS line approached this region, SST
399 decreased at a rate of $-0.22 \pm 0.06^\circ\text{C y}^{-1}$ (Fig. 3). Solely, this decrease in temperature
400 would increase the pH by a rate of $+0.004 \text{ yr}^{-1}$ and the $f\text{CO}_2$ would decrease by $4 \mu\text{atm yr}^{-1}$



401 ¹ The net effect of the increase in the amount of rich CO₂/low pH upwelled waters in the
 402 Mauritanian upwelling would be, therefore, a decrease in the pH of over -0.007 ± 0.002
 403 units y⁻¹ and an increase in $f\text{CO}_2$ of $+6.5 \pm 0.7 \mu\text{atm y}^{-1}$ (with periods where those rates
 404 could reach values of 0.015 y^{-1} in pH and $10.5 \mu\text{atm y}^{-1}$ in $f\text{CO}_2$ as recorded during 2005-
 405 2008). Those values are greatly compensated by the important decrease in the SST
 406 resulting in the observed rates of -0.003 ± 0.001 pH units and $+2.5 \pm 0.4 \mu\text{atm}$ of $f\text{CO}_2$
 407 per year.



408 Fig. 6. pH at *in situ* SST in total proton scale computed from total alkalinity (based on regional
 409 correlations with SST and SSS, Lee et al., 2006) and $f\text{CO}_2$ at $21 \pm 0.25^\circ\text{N}$. The error bar represents
 410 the standard deviation of the computed data for each cruise for the selected latitude. The black
 411 line shows the harmonic fitting Eq. (3) for the data and the corresponding linear trend.

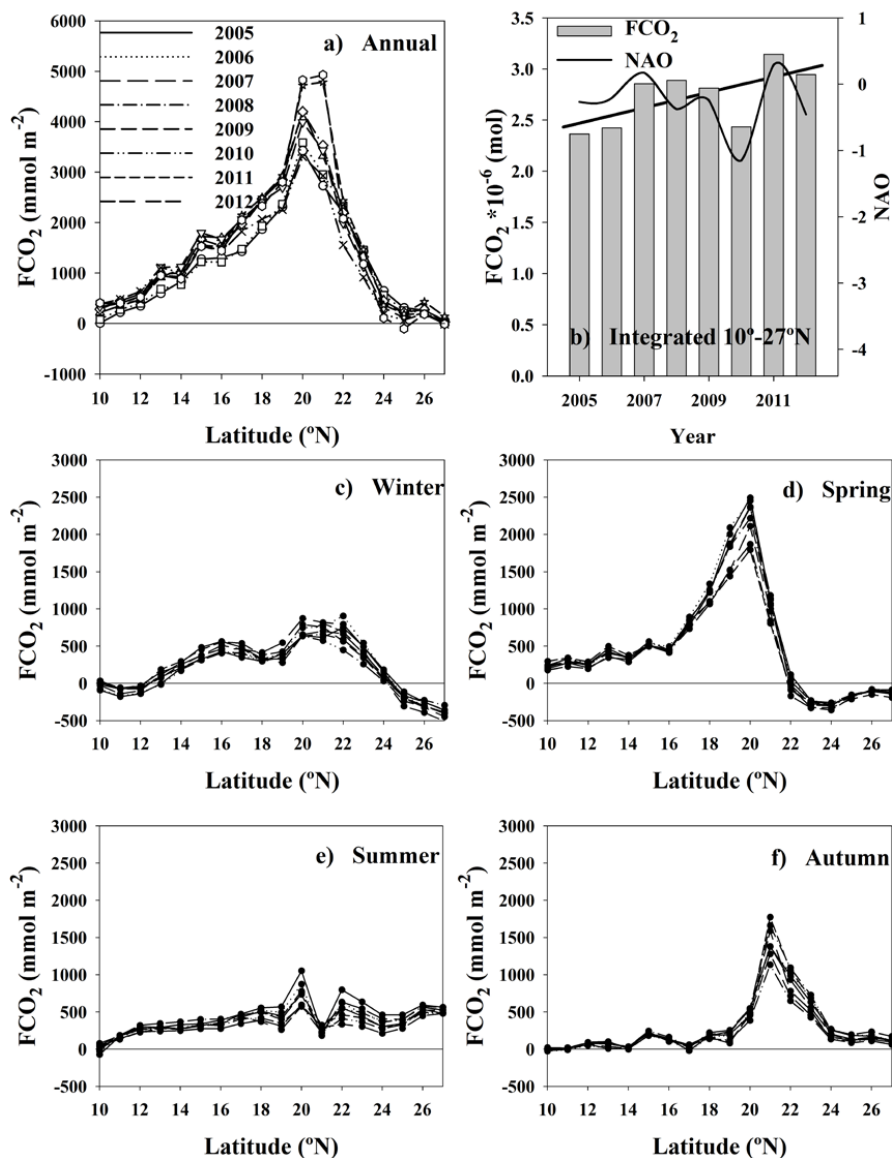
412

413

414 3.3 Fluxes of CO₂

415 The annual air-sea CO₂ flux for the full domain was positive (Fig. 7a), with the area off

416 Mauritania, between 18 and 22°N, acting as an active source of CO₂ to the atmosphere



417 Fig. 7. Latitudinal distribution of seasonal and annual CO₂ fluxes, FCO₂ (mmol m⁻²). Fluxes of
 418 CO₂ were computed using Wanninkhoff (1992) parametrization and satellite winds with a
 419 resolution of 6 hours. a) Integrated year-to-year from 2005 to 2012 and b) latitudinally integrated
 420 for 2005 to 2012 together with annual values for NAO index. Latitudinal distribution of FCO₂
 421 seasonally integrated from 2005 to 2012 are depicted for winter (c), spring (d), summer (e) and
 422 autumn (f).
 423

424 with values close to 5 mol CO₂ m⁻² (Fig. 7a). North of 24°N, in the area not affected by
 425 the coastal upwelling, an average flux of $+0.2 \pm 0.1$ mol CO₂ m⁻² was determined.



426 The ingassing observed during winter and spring of -185 ± 36 mmol CO₂ m⁻² for the full
427 period (Fig. 7) was surpassed by the outgassing during summer and autumn of 295 ± 150
428 mmol CO₂ m⁻². South of 24°N, it was observed that during spring (Fig. 7d) the
429 photosynthetic activity was not intense enough to uptake the CO₂ injected by the strongest
430 upwelling in the surface waters and the area acted as a source of CO₂ with values reaching
431 3 mol CO₂ m⁻² in 2012. During summer (Fig. 7e), primary producers and lateral advection
432 of warm waters by the Mauritanian current could consume/export the CO₂ rich waters
433 reaching values of 0.5 mol m⁻². During autumn (Fig. 7f), only the area between 20°N and
434 23°N acted as a source of 1-2 mol CO₂ m⁻², while the rest was almost in equilibrium. It
435 was also detected that the late autumn-winter upwelling in the 14° to 17°N region
436 contributed to an increased outgassing with a second annual submaximum of about 0.7
437 mol CO₂ m⁻² in winter (Fig. 7c). South of 14°N, annual CO₂ fluxes decreased from about
438 1 mol m⁻² at 14°N to being roughly in equilibrium at 10°N.

439 The integrated CO₂ fluxes for the area 10° to 27°N along the VOS line section for
440 the years 2005 to 2012 (Fig. 7b) were between 2.3 and 3.1 10⁶ mol, with an important
441 interannual variability. FCO₂ increased during the studied period by $0.08 \pm 0.03 \cdot 10^6$ mol
442 yr⁻¹. The augment in FCO₂ is related to the observed increase in wind speed (Fig. 3,
443 indicated as UI) north of 16°N that far surpassed the effect of the smaller annual rate of
444 increase in $f\text{CO}_2^{\text{sw}}$ than in $f\text{CO}_2^{\text{atm}}$ north of 19°N with the exception at 21°N (Fig. 3). South
445 of 16°N, the decrease in wind speed did not exceed the effect of the increment in $\Delta f\text{CO}_2$
446 associated to the increase in downwelling indexes (Fig. 3; Santos et al., 2012), and FCO₂
447 was slightly ascending. The variability observed in the annual integrated CO₂ fluxes (Fig.
448 7b) was related with the basin-scale oscillations, the North Atlantic Oscillation (NAO)
449 index and the East-Atlantic Pattern (EA)
450 (<http://www.cpc.ncep.noaa.gov/data/teledoc/telecontents.shtml>). Cropper et al. (2014)



451 found winter upwelling variability was strongly correlated with the winter NAO (r values
452 ranged from 0.50 at 12–19°N to 0.59 at 21–26°N), due to the strength of the Azores semi-
453 permanent high-pressure system, which modifies trade wind strengths. The annual
454 integrated fCO_2 was related with the annual NAO index (Fig. 7b) with a similar $r = 0.54$,
455 even when fluxes are not only controlled by wind strength. However, Fig. 7a clearly
456 indicates that the Mauritanian upwelling area was the most important contributor to
457 fCO_2 . There was not a significant correlation coefficient with the winter NAO ($r = 0.23$).
458 Also, the EA index, because represents the southward-shifted NAO-like oscillation,
459 presented a lower significant value ($r = 0.48$), as it was observed by the upwelling index
460 (Cropper et al., 2014). The correlation between fluxes and climate indexes describing the
461 main mode of variability across the Atlantic sector may be directly related to the Azores
462 High and its influence on the trade wind strength.

463 If the fCO_2 values are assumed to be valid for at least 100 km to both sides of the
464 QUIMA-VOS line, the total flux of CO_2 being ejected to the atmosphere would reach a
465 value of 30 Tg of carbon dioxide a year for the period 2005-2012, with a rate of increase
466 of 1 Tg yr^{-1} . However, it should be considered that the export of the rich fCO_2 upwelled
467 water with high nutrient concentration off the coastal areas would promote a decrease in
468 surface fCO_2 values (as those observed north and south 21°N) that will produce an
469 ingassing of CO_2 . This could balance the observed outgassing increase in a more global
470 scale.

471

472 4. CONCLUSIONS

473 The Mauritanian-Cape Verde upwelling has been shown to be an important area sensitive
474 to decadal and climate change forcing on upwelling processes, which strongly affects the
475 CO_2 surface distribution, ocean acidification rates and air-sea CO_2 exchange.



476 The results for the period 2005 to 2012 confirm, firstly, the upwelling intensification at
477 the Mauritanian-Cape Verde upwelling system by using experimental SST and carbon
478 dioxide system variables. Secondly, that upwelling regions at low-mid latitudes are strong
479 sources of CO₂ to the atmosphere and thirdly, that as a direct result, the pH is decreasing
480 at a rate of -0.003 ± 0.001 per year and the amount of emitted CO₂ is increasing annually
481 at a rate of 1 Tg due to wind increase even when primary production seems to also be
482 reinforced in the upwelling area. The extent to which those changes can be attributed to
483 natural decadal variability in this EBUS over interannual timescales remains unclear and
484 more years of monthly data should be recorded. Sustained volunteer observing lines are
485 shown as one of the most significant contributors to the knowledge of how ocean
486 surface waters are being affected by present and future climate change. The results from
487 VOS lines can provide accurate data for changes in SST, FCO₂ and, consequently,
488 upwelling intensification effects due to global change conditions under decadal natural
489 variability.
490



491 **Data availability.**

492 All data are free available at the SOCAT data base, <http://www.socat.info/> and at the
493 Carboocean and Carbochange web pages www.CarboOcean.org,
494 <https://carbochange.b.uib.no/>, respectively

495
496

497 **Team List**

498 Melchor Gonzalez Davila, Professor of Marine Chemistry at the University of Las Palmas
499 de Gran Canaria. Melchor.gonzalez@ulpgc.es

500 J. Magdalena Santana Casiano, Professor of Chemical Oceanography at the University of
501 Las Palmas de Gran Canaria. Magdalena.santana@ulpgc.es

502 Francisco Machin, Associated Professor of Physical Oceanography at the University of
503 Las Palmas de Gran Canaria. Francisco.machin@ulpgc.es

504

505 **Author contributions**

506 M.G.D. and J.M.S.C worked in the equipment installation, data collection and designed
507 the study. F.M. processed the data, generated figures and results. All of them collaborated
508 in the discussion of the data and the writing of the paper.

509

510 **Competing interests**

511 There is not any competing interest.

512

513

514 **Acknowledgements**

515 Financial support from the European Union through the Integrated Project FP6

516 CarboOcean under grant agreement no. 511106-2 and FP7 project CARBOCHANGE

517 under grant agreement no. 264879 are gratefully acknowledged. Special thanks go to the



518 Mediterranean Shipping Company (MSC) (years 2005- 2008) and the Maersk Company
519 (years 2010-2013) who provided the ship platforms and scientific facilities. The Modis-
520 Aqua Ocean Color Data, 2005-2012 reprocessing, NASA OB.DAAC, Greenbelt, MD,
521 USA is strongly acknowledged.
522



523 **References**

524

525 Astor, Y., Scranton, M., Muller-Karger, F., Bohrer, R. n and Garcia, J.: CO₂ variability
526 at the CARIACO tropical coastal upwelling time series station, *Mar. Chem.*, 97(3), 245–
527 261, 2005.

528 Bakun, A.: Global climate change and intensification of coastal ocean upwelling, *Science*,
529 247(4939), 198–201, 1990.

530 Barton, E. D., Field, D.B., and Roy, C.: Canary current upwelling: More or less?, *Prog.*
531 *Oceanogr.*, 116, 167-178, 2013.

532 Bates, N. R., Astor, Y. M., Church, M. J., Currie, K., Dore, J. E., González-Dávila, M.,
533 Lorenzoni, L., Muller-Karger, F., Olafsson, J., and Santana-Casiano, J. M.: A time-series
534 view of changing ocean chemistry due to ocean uptake of anthropogenic CO₂ and ocean
535 acidification, *Oceanography* 27(1), 126–141, doi:10.5670/oceanog.2014.16, 2014.

536 Borges, A. V., and Frankignoulle, M.: Distribution of surface carbon dioxide and air-sea
537 exchange in the upwelling system off the Galician coast, *Global Biogeochem. Cycles*,
538 16(2), 1020, doi:10.1029/2000GB001385, 2002.

539 Borges, A. V., Delille, B., and Frankignoulle, M.: Budgeting sinks and sources of CO₂ in
540 the coastal ocean: Diversity of ecosystems counts, *Geophys. Res. Letters*, 32, L14601,
541 doi:10.1029/2005GL023053, 2005.

542 Cai, W.-J., Dai, M., Wang, Y.: Air–sea exchange of carbon dioxide in ocean margins:
543 a province-based synthesis, *Geophys. Res. Lett.*, 33, L12603,
544 doi:10.1029/2006GL026219, 2006.

545 Chen, C. T. - A., Huang, T. -H., Chen, Y. C., Bai, Y., He, X., and Kang, Y.: Air-sea
546 exchanges of CO₂ in the world's coastal seas, *Biogeosciences*, 10, 6509-6544,
547 doi:10.5194/bg-10-6509-2013, 2013.

548 Cropper, T. E., Hanna, E., and Bigg, G. R.: Spatial and temporal seasonal trends in coastal
549 upwelling off Northwest Africa, 1981–2012, *Deep-Sea Res. I*, 86, 94–111, 2014.

550 Demarcq, H.: Trends in primary production, sea surface temperature and wind in
551 upwelling systems (1998–2007), *Prog. Oceanogr.*, 83, 376–385,
552 doi:10.1016/j.pocean.2009.07.022, 2009.

553 Dickson, A. G., Millero, F. J.: A comparison of the equilibrium constants for the
554 dissociation of carbonic acid in seawater media, *Deep-Sea Res.*, 34, 1733–1743, 1987.



- 555 DOE. Handbook of methods for the analysis of the various parameters of the carbon
556 dioxide system in sea water, ORNL/CDIAC-74,
557 <http://cdiac.ornl.gov/oceans/handbook.html>, 1994 (date of access 07/03/2017)
- 558 Dore, J. E., Lukas, R. , Sadler, D. W., and Karl, D. M.: Climate-driven changes to the
559 atmospheric CO₂ sink in the subtropical North Pacific Ocean, *Nature*, 424(6950), 754–
560 757, 2003.
- 561 Feely, R. A., Boutin, J., Cosca, C. E., Dandonneau, Y., Etcheto, J., Inoue, H. Y., Ishii, M.
562 , Quéré, C. L., Mackey, D. J., McPhaden, M., Metzl, N., Poisson, A., and Wanninkhof,
563 R.: Seasonal and interannual variability of CO₂ in the equatorial Pacific, *Deep Sea Res.*
564 II, 49(13), 2443–2469, 2002.
- 565 Feely, R.A., Sabine, C. L., Hernandez-Ayon, J.M., Ianson, D., and Hales, B.: Evidence
566 for upwelling of corrosive ‘acidified’ water onto the continental shelf, *Science*, 320
567 (5882), 1490–1492, doi:10.1126/science.1155676, 2008.
- 568 Frankignoulle, M., and Borges, A. V.: European continental shelf as a significant sink for
569 atmospheric carbon dioxide, *Global Biogeochem. Cycles*, 15(3), 569–576, 2001.
- 570 Friederich, G. E., Ledesma, J., Ulloa, O., and Chavez, F. P.: Air-sea carbon dioxide fluxes
571 in the coastal southeastern tropical Pacific, *Prog. Oceanogr.*, 79(2-4), 156 – 166, 2008.
- 572 González Dávila, M., Santana-Casiano, M. J., Merlivat, L., Barbero-Munoz, L., and
573 Dafner, E.: Fluxes of CO₂ between the atmosphere and the ocean during the POMME
574 project in the northeast Atlantic Ocean during 2001, *J. Geophys. Res.*, 110(C7), C07S11,
575 2005.
- 576 González-Dávila, M., Santana-Casiano, J. M., and Ucha, I.: Seasonal variability of fCO₂
577 in the Angola-Benguela region, *Prog. Oceanogr.*, 83, 124–133, 2009.
- 578 González-Dávila, M., Santana-Casiano, J. M., Rueda, M., and Llinás, O.: The water
579 column distribution of carbonate system variables at the ESTOC site from 1995 to 2004,
580 *Biogeosciences*, 7, 3067-3081, 2010.
- 581 Gruber, N. Warming up, turning sour, losing breath: ocean biogeochemistry under global
582 change, *Philos. Trans. R. Soc. London, Ser. A*, 369 (1943), 1980–1996, 2011.
- 583 Gruber, N., Keeling, C. D., and Bates, N. R.: Interannual variability in the North Atlantic
584 Ocean carbon sink, *Science*, 298(5602), 2374–2378, 2002.
- 585 Hagen, E., Schemainda, R. Der Guineadom im ostatlantischen Stromsystem, *Beitr.*
586 *Meereskd.*, 51, 5–27, 1984.
- 587 Hales, B., Takahashi, T., and Bandstra, L.: Atmospheric CO₂ uptake by a coastal
588 upwelling system, *Global Biogeochemical Cycles*, 19(1), GB1009, 2005.



- 589 Keeling, R. F., Kortzinger, A., and Gruber, N.: Ocean deoxygenation in a warming world,
590 *Annu. Rev. Mar. Sci.*, 2, 199–229; doi:10.1146/annurev.marine.010908.163855, 2010.
- 591 Key, R., Kozyr, A., Sabine, C., Lee, K., Wanninkhof, R., Bullister, J., Feely, R., Millero,
592 F. J., Mordy, C., and Peng, T. - H.: A global ocean carbon climatology: Results from
593 GLODAP, *Global Biogeochem. Cycles*, 18, GB4031, 2004.
- 594 Lachkar, Z., and Gruber, N.: Response of biological production and air–sea CO₂ fluxes
595 to upwelling intensification in the California and Canary Current Systems, *J. Mar. Sys.*,
596 109–110, 149–160, 2013.
- 597 Lee, K., Tong, L. T., Millero, F. J., Sabine, C. L., Dickson, A. G., Goyet, C., Park, G. H.,
598 Wanninkhof, R., Feely, R. A., and Key, R. M.: Global relationships of total alkalinity
599 with salinity and temperature in surface waters of the world’s oceans, *Geophys. Res. Lett.*
600 33, L19605, doi:10.1029/2006GL027207, 2006.
- 601 Lüger, H., Wallace, D. W., Körtzinger, A., and Nojiri, Y.: The pCO₂ variability in the
602 midlatitude North Atlantic Ocean during a full annual cycle, *Global Biogeochem. Cycles*,
603 18(3), GB3023, doi:10.1029/2003GB002200, 2004.
- 604 Lüger, H., Wanninkhof, R., Wallace, D. W., and Körtzinger, A.: CO₂ fluxes in the
605 subtropical and subarctic North Atlantic based on measurements from a volunteer
606 observing ship, *J. Geophys. Res.*, 111, C06024, doi:10.1029/2005JC003101, 2006.
- 607 Marcello, J., Alonso, H., Eugenio, F., and Fonte, A., Seasonal and temporal study of the
608 northwest African upwelling system, *Int. J. Remote Sens.*, 32:7, 1843-1859,
609 doi:10.1080/01431161003631576, 2011.
- 610 Mehrbach, C., Culberson, C. H., Hawley, J. E., Pytkowicz, R. N.: Measurement of the
611 apparent dissociation constants of carbonic acid in seawater at atmospheric pressure,
612 *Limnol. Oceanogr.*, 18, 897–907, 1973.
- 613 Michaels, A. F., Karl, D. M., and Capone, D. G.: Element stoichiometry, new production
614 and nitrogen fixation, *Oceanography*, 14(4), 68–77, 2001.
- 615 Mittelstaedt, E.: The upwelling area off Africa—A description of phenomena related to
616 coastal upwelling, *Prog. Oceanogr.*, 12, 307–331, doi:10.1016/0079-6611(83)90012-5.,
617 1983.
- 618 Neuer, S., Torres-Padrón, M. E., Gelado-Caballero, M. D., Rueda, M. J., Hernández-
619 Brito, J. J., Davenport, R., and Wefer, G.: Dust deposition pulses to the eastern subtropical
620 North Atlantic gyre: Does ocean's biogeochemistry respond?, *Global Biogeochem.*
621 *Cycles*, 18, GB4020, doi:10.1029/2004GB002228, 2004.



- 622 Nicholson, S. E.: Rainfall and atmospheric circulation during drought periods and wetter
623 years in West Africa, *Monthly Weather Review*, 109(10), 2191–2208, 1981.
- 624 Nykjaer, L., and Van Camp, L.: Seasonal and interannual variability of coastal upwelling
625 along Northwest Africa and Portugal from 1981 to 1991, *J. Geophys. Res.*, 99, 14197–
626 14207, 1994.
- 627 Oerder, V., Colas, F., Echevin, V., Codron, F., Tam, J., and Belmadani, A.: Peru-Chile
628 upwelling dynamics under climate change, *J. Geophys. Res. Ocean*, 120, 1152–1172,
629 doi:10.1002/2014JC010299, 2015.
- 630 Padín, X., Vázquez-Rodríguez, M., Castaño, M., Velo, A., Alonso-Pérez, F., Gago, J.,
631 Gilcoto, M., Álvarez, M., Pardo, P., de La Paz, M., Rios, A. F., and Perez, F.F.: Air-Sea
632 CO₂ fluxes in the Atlantic as measured during boreal spring and autumn, *Biogeosciences*,
633 7, 1587–1606, 2010.
- 634 Quan, X. W., Diaz, H. F., and Hoerling, M. P.: Change of the Tropical Hadley Cell Since
635 1950, In: *The Hadley Circulation: Past, Present, and Future*, edited by Diaz, H. F., and
636 Bradley, R. S., , Kluwer Academic Publishers, New York, 85–120, 2004.
- 637 Santana-Casiano, J., González-Dávila, M., and Ucha, I.: Carbon dioxide fluxes in the
638 Benguela upwelling system during winter and spring: A comparison between 2005 and
639 2006, *Deep Sea Res. II*, 56(8), 533–541, 2009.
- 640 Santana-Casiano, J., González-Dávila, M., Rueda, M., Llinás, O., and González-Dávila,
641 E- F.: The interannual variability of oceanic CO₂ parameters in the northeast Atlantic
642 subtropical gyre at the ESTOC site, *Global Biogeochem. Cycles*, 21(1), GB1015,
643 doi:10.1029/2006GB002788, 2007.
- 644 Santos, A.M.P., Kazmin, A.S., and Peliz, A.: Decadal changes in the Canary upwelling
645 system as revealed by satellite observations: Their impact on productivity, *J. Mar. Res.*,
646 63, 359–379, 2005.
- 647 Santos, F., de Castro, M., Gómez-Gesteira, M., and Alvarez, I.: Differences in coastal and
648 oceanic SST warming rates along the Canary upwelling ecosystem from 1982 to 2010,
649 *Continental Shelf Res.*, 47, 1–6, 2012.
- 650 Schuster, U., Watson, A., Bates, N., Corbiere, A., Gonzalez-Davila, M., Metzl, N.,
651 Pierrot, D., and Santana-Casiano, J.M.: Trends in North Atlantic sea-surface fCO₂ from
652 1990 to 2006, *Deep Sea Res. II*, 56(8), 620–629, 2009.
- 653 Takahashi, T., Olafsson, J., Goddard, J. G., Chipman, D. W., and Sutherland, S.: Seasonal
654 variation of CO₂ and nutrients in the high-latitude surface oceans: A comparative study,
655 *Glob. Biogeochem. Cycles*, 7(4), 843–878, 1993.



656 Takahashi, T., Sutherland, S., Wanninkhof, R., Sweeney, C., Feely, R., Chipman, D.,
657 Hales, B., Friederich, G., Chavez, F., Sabine, C., Watson, A., Bakker, D., Schuster, U.,
658 Metzl, N., Yoshikawa-Inoue, H., Ishii, M., Midorikawa, T., Nojiri, Y., Kortzinger, A.,
659 Steinhoff, T., Hoppema, M., Olafsson, J., Arnarson, T., Tilbrook, B., Johannessen, T.,
660 Olsen, A., Bellerby, A., Wong, C., Delille, B., Bates, N., and de Baar, H.: Climatological
661 mean and decadal change in surface ocean pCO₂, and net sea-air CO₂ flux over the global
662 oceans, *Deep-Sea Res. II*, 56(8-10), 554–577, 2009.

663 Ullman, D. J., McKinley, G. A., Bennington, V., and Dutkiewicz, S.: Trends in the North
664 Atlantic carbon sink: 1992–2006, *Glob. Biogeochem. Cycles*, 23(4),
665 doi:10.1029/2008GB003383, 2009.

666 Varela, R., Álvarez, I., Santos, F., de Castro, M., Gómez-Gesteira, M.: Has upwelling
667 strengthened along worldwide over 1982-2010?, *Sci. Rep.* 5, 10016;
668 doi:10.1038/srep10016, 2015.

669 Wang, Y., Castelao, R. M., and Yuan, Y.: Seasonal variability of alongshore winds and
670 sea surface temperature fronts in Eastern Boundary Current Systems, *J. Geophys. Res.*
671 *Oceans*, 120, 2385–2400; doi:10.1002/2014JC010379, 2015.

672 Wanninkhof, R.: Relationship between wind speed and gas exchange over the ocean, *J.*
673 *Geophys. Res.*, 97, 7373-7382, 1992.

674 Watson, A., Schuster, U., Bakker, D., Bates, N., Corbière, A., González-Dávila, M.,
675 Friedrich, T., Hauck, J., Heinze, C., Johannessen, T., Kortzinger, A., Metzl, N., Olafsson,
676 J., Olsen, A., Oschlies, A., Padin, X. A., Pfeil, B., Santana-Casiano, J. M., Steinhoff, T.,
677 Telszewski, M., Rios, A. F., Wallace, D. W., and Wanninkhof, R.: Tracking the variable
678 North Atlantic sink for atmospheric CO₂, *Science*, 326(5958), 1391–1393,
679 doi:10.1126/science.1177394, 2009.

680 Yoo, J.-M. and Carton, J. A.: Annual and interannual variation of the freshwater budget
681 in the tropical Atlantic Ocean and the Caribbean Sea, *J. Phys. Oceanogr.*, 20(6), 831–845,
682 1990.

683